Bioorganic & Medicinal Chemistry 22 (2014) 95–104

Contents lists available at ScienceDirect

Bioorganic & Medicinal Chemistry

journal homepage: www.elsevier.com/locate/bmc

A highly predictive 3D-QSAR model for binding to the voltage-gated sodium channel: Design of potent new ligands

Congxiang Zha [a], George B. Brown [b], Wayne J. Brouillette [a,*]

[a] Department of Chemistry, The University of Alabama at Birmingham, Birmingham, AL 35294, United States
[b] Department of Psychiatry and Behavioral Neurobiology, The University of Alabama at Birmingham, Birmingham, AL 35294, United States

ARTICLE INFO

Article history:
Received 15 September 2013
Revised 17 November 2013
Accepted 25 November 2013
Available online 6 December 2013

Keywords:
Sodium channel
CoMFA model
Nanomolar ligands

ABSTRACT

A comprehensive comparative molecular field analysis (CoMFA) model for the binding of ligands to the neuronal voltage-gated sodium channel was generated based on 67 diverse compounds. Earlier published CoMFA models for this target provided μM ligands, but the improved model described here provided structurally novel compounds with low nM IC_{50}. For example, new compounds **94** and **95** had IC_{50} values of 129 and 119 nM, respectively.

1. Introduction

Voltage-gated sodium channels (VGSCs) are responsible for the generation of conducted electrical signals in neurons and other excitable cells.[1–5] Upon polarization, the permeability of the cell membrane to sodium ions increases dramatically over a period of 0.5 to hundreds of msec and then decreases to the baseline level over a period of 2 ms to a few seconds. This biphasic behavior results from two experimentally separable gating processes that control ion channel function: activation, which controls the rate and voltage dependence of the permeability increase following depolarization, and inactivation, which controls the rate and voltage dependence of the subsequent return of the ion permeability to the resting level during a maintained depolarization.

The properties of the sodium channel have been shown to be important for several physiological and pathological functions.[6–8] It not only is responsible for the initiation and conduction of neuronal action potentials but can also influence neurotransmitter release from presynaptic vesicles. Furthermore, the maintenance of ionic homeostasis of neurons is the basis for normal functions; thus, any improper transportation of sodium ions can cause neurons to malfunction. Meanwhile, in neuronal preparations very small persistent Na^+ currents arise from sustained or repeated Na^+ channel openings. These persistent currents last much longer than the 1–5-ms duration of action potentials.[5] It is likely that the persistent current is involved with the repeated depolarizing waves associated with seizures, spreading depression and the sustained depolarization of ischemic brain tissues. Therefore, drugs that selectively block voltage-sensitive Na^+ channels (particularly persistent Na^+ currents) are a reasonable choice for treating epilepsy, stroke, cerebral ischemia, and head trauma. Sodium channels have also been targeted for the design of numerous other drugs, including local anesthetics, class I antiarrhythmics, anticonvulsants which have a pharmacological profile like that of diphenylhydantoin (DPH, or phenytoin), analgesics, and neuroprotective agents.[9–17]

While VGSCs are well recognized to exist in excitable tissues such as nerve and muscle, in the past fifteen years they have been found in non-excitable tissues, including a broadening number of aggressive metastatic cancers,[18] but they are not found in nonaggressive cancers or normal tissue. A growing body of evidence suggests that VGSCs play an important pathological role during cancer progression toward metastasis. Their role in regulating cellular migration and invasion, and their potential utility as diagnostic and therapeutic targets has drawn increasing attention. In fact, known drugs that target sodium channels such as anticonvulsants, local anesthetics, and antiarrhythmics have been observed to significantly reduce the metastasis of tumor cells.[19–24] The diverse and growing number of important applications for this channel as a drug target emphasizes the need for efficient drug design methodologies.

In contrast to the widely and thoroughly studied physiological and pharmacological properties of the sodium channel, the 3-dimensional (3-D) structure of the binding site is much less understood due to difficulties in crystallizing the high molecular weight transmembrane protein from mammalian cells. Historically, design of drugs for sodium channel-related diseases has been carried out

* Corresponding author. Tel.: +1 205 934 8288.
E-mail address: wbrou@uab.edu (W.J. Brouillette).

0968-0896/$ - see front matter © 2013 Elsevier Ltd. All rights reserved.
http://dx.doi.org/10.1016/j.bmc.2013.11.049

largely by screening compound arrays. 3-D QSAR models generated from activities of known compounds are attractive alternatives to assist medicinal chemists in rational drug design when crystal structures of protein targets are not available. The utility of such models lies in their ability to accurately predict the biological activities for newly designed ligands.

In a previous paper[25] we developed a preliminary 3-D QSAR (comparative molecular field analysis, or CoMFA) model for the binding of ligands to the sodium channel that was trained using a group of 5-phenylhydantoins. However, this model is highly limited since only a single class of compounds (hydantoins) was included in the training set, which can probe only limited 3 dimensional steric and electrostatic space. To evaluate further the importance of the hydantoin ring, and to explore spatial features of related non-hydantoin compounds to increase structural diversity, we previously reported a number of new types of sodium channel ligands and a systematic SAR study for these compounds.[26] The results suggest that the high potency of ligands for this channel may result from the contribution of distinct hydrophobic groupings: two phenyl groups at the 5-position of the hydantoin ring and a hydrophobic substituent at the *N*-3 position. This also suggests that further spatial information beyond the existing pharmacophore needs to be uncovered.

Recently, Brown and co-workers published two CoMFA models for the neuronal voltage-gated sodium channel.[27,28] In one model, the authors combined the pharmacophore of the CoMFA model generated by using a group of hydantoins as the training set, and the scaffold of propofol, for new design. In the other model, the authors combined the pharmacophore of local anesthetics, hydantoins and hydroxyphenylamides. These models offer new insights about the binding of the blockers to the channel, but the most potent newly designed compounds based on the models were micromolar blockers. As for most drug targets, it is desirable to develop models that can be used to design ligands with IC_{50} values at the low nanomolar or better level.

To achieve this goal, we proposed to develop a more comprehensive 3-D QSAR model that can include structural information associated with a much greater variety of structural types and drug

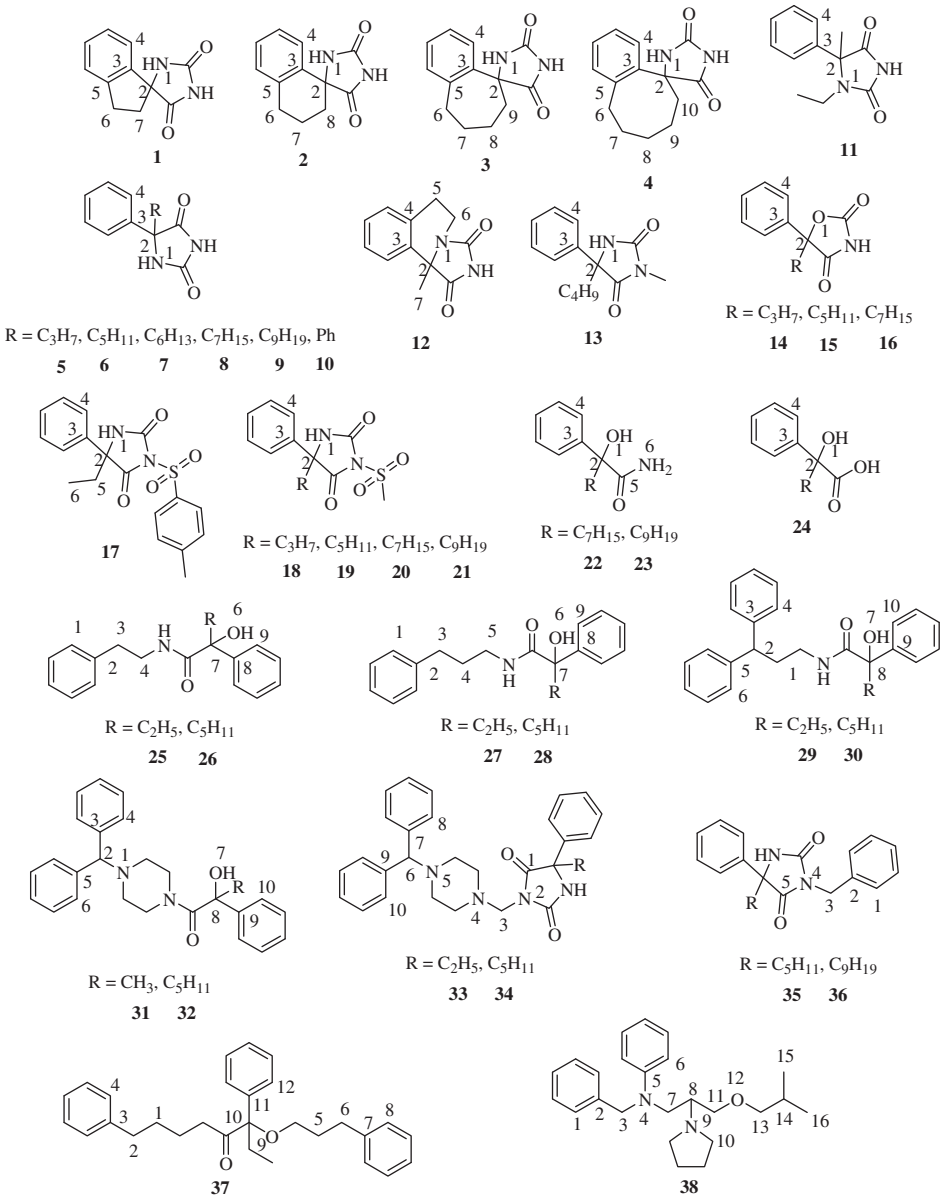

Figure 1. Compounds used in the training set.

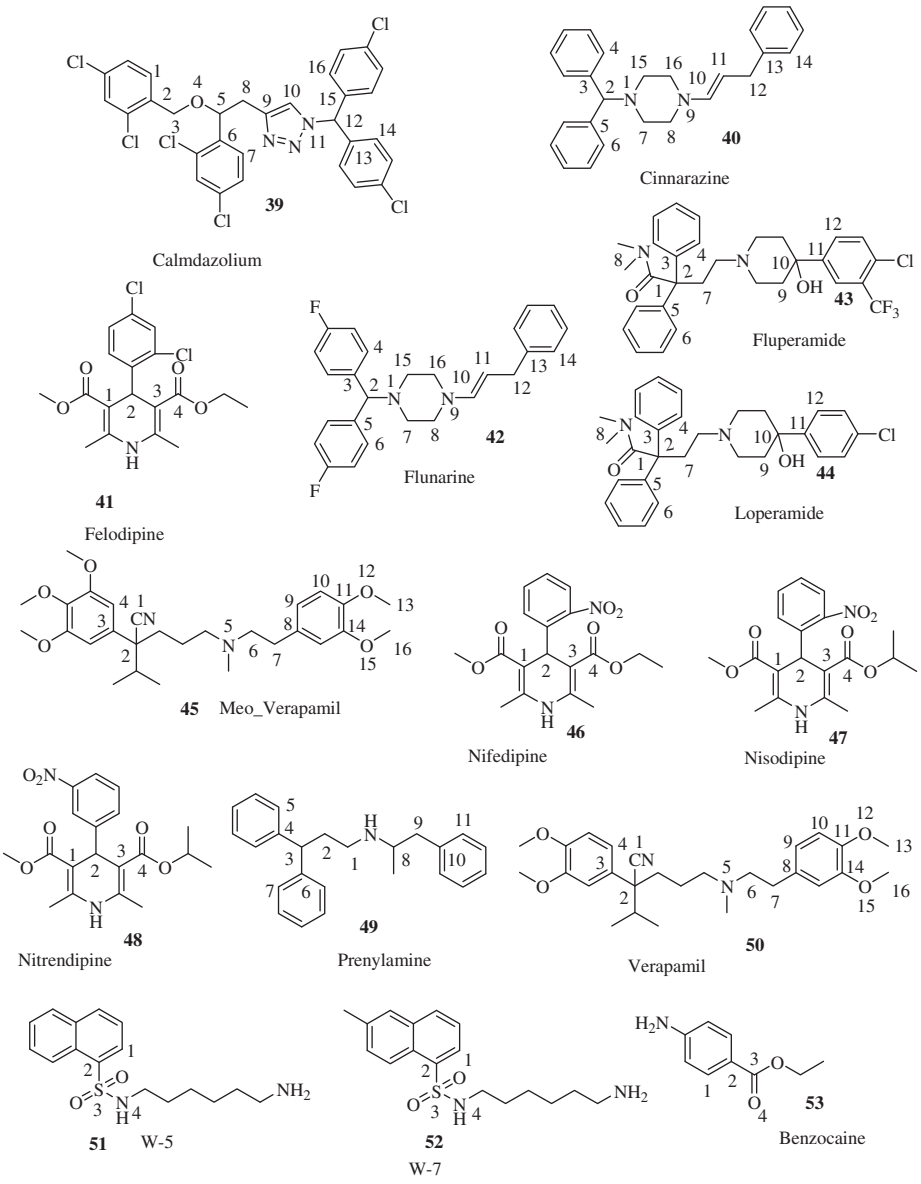

Fig. 1 (*continued*)

classes that all bind to the sodium channel. This includes local anesthetics, anticonvulsants, and antiarrhythmics, which have been proposed to bind to the same receptor site.[29–34] In the present study we used a training set of 67 sodium channel blockers, 36 of which were synthesized in our laboratory and 31 sodium channel blockers from the literature.[35] Of the 31 compounds from the literature, 15 compounds are local anesthetics, one is the anticonvulsant DPH, and the other 15 compounds are Ca^{2+} and Na^{+} channel mixed blockers (Fig. 1). The dependent variable is the IC_{50} value obtained using the [^{3}H]batrachtoxinin A 20-α-benzoate ([^{3}H]BTX-B) sodium channel binding assay. All of the literature compounds were taken from a single literature reference[36] that used the same [^{3}H]BTX-B binding assay that we employed. It was anticipated that data obtained using similar assays would reduce errors in the model. CoMFA calculations were then carried out to correlate the effects of changes in steric and electrostatic effects for the 67 compounds in the database. We describe here the resulting high-quality model and its utility in designing new potent ligands with low nanomolar IC_{50} values.

2. Methods

2.1. Biological data

In the sodium channel evaluation, the IC_{50}, which represents the concentration of compound required to displace 50% of specifically bound [^{3}H]BTX-B, was determined in an in vitro assay using rat brain cerebral cortex synaptoneurosomes. For each IC_{50} value, 5–7 concentrations (triplicate determinations) were used. The IC_{50} value was obtained from a Probit analysis of the data that plots the log concentration versus the Probit number (converted from percent binding of [^{3}H]BTX-B for the samples). The concentration where the Probit number equals 5 is the IC_{50} value. The activities of compounds from the literature were obtained using an identical

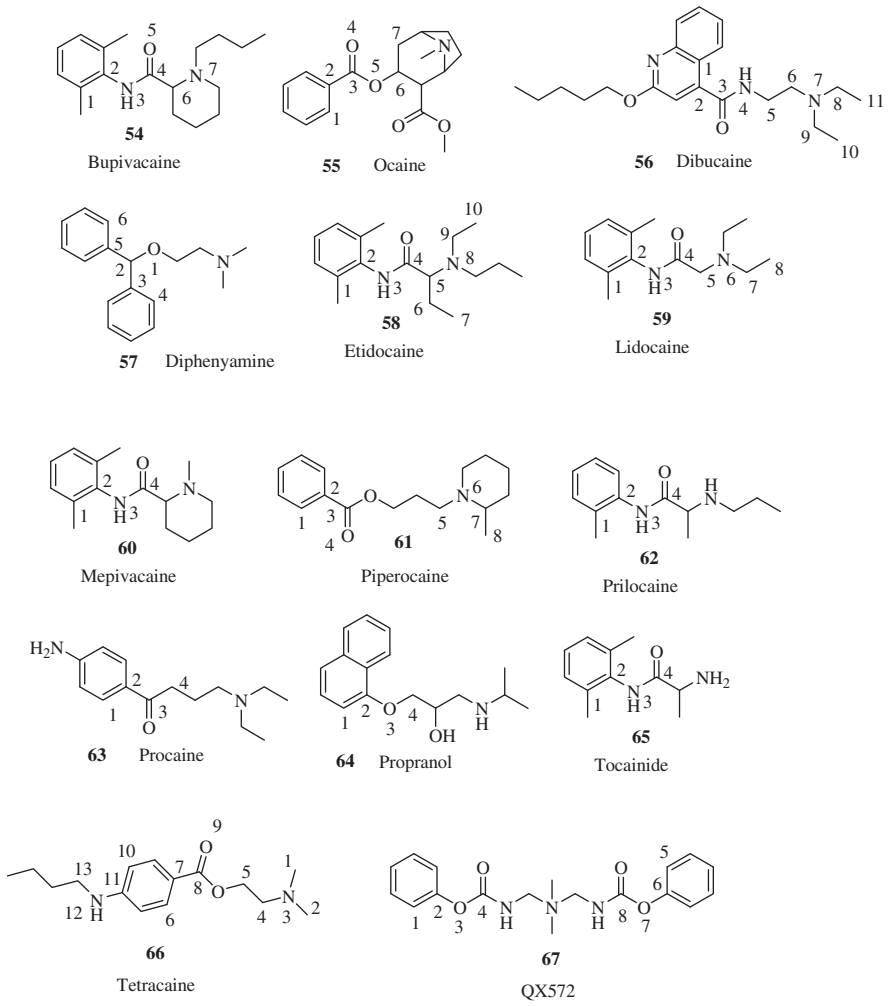

Fig. 1 (*continued*)

binding assay, which gave the same value for DPH (IC_{50} = 40 μM) obtained in the present assay.

2.2. Conformational search

All conformational searches were performed on a SGI Octane using SYBYL software (Tripos Assoc., Inc.). In conformational searches, two assumptions were made: (1) all molecules are in a fully extended conformation, and (2) all chiral centers are R unless the actual configuration was known. Based on the first assumption, if a molecule had ring system(s) which belong to part of the extended chain between two ends of the molecule, extended conformations which contain part of the ring system were used if they belonged to the lowest energy conformations (within 2 kcal/mol of the global energy minimum). For compounds containing the diphenylmethyl fragment, only one low-energy conformation was used for the diphenylmethyl group. For compounds with a terminal phenyl ring, the conformation with the phenyl ring orientation corresponding to one of the two phenyl groups in the diphenylmethyl compounds was included in the analysis. No conformations that had conformational energy >2 kcal/mol above the global energy minimum were considered. Based on these assumptions and definitions, conformational searches using the 'grid search' and 'random search' routines of SYBYL were performed with the remaining rotatable bonds. The chemical structures of the training set are shown in Figure 1, and lowest conformations of the training set used in this study are listed in Table 1S (Supplementary data). See Supplementary data—conformational search and alignment for details.

2.3. CoMFA calculation

CoMFA, using default parameters except where noted, was calculated in the QSAR option of SYBYL 6.4 on the SGI Octane computer. The CoMFA grid spacing was 2.0 Å in the *x*, *y* and *z* directions, and the grid region was automatically generated by the CoMFA routine to encompass all molecules with an extension of 4.0 Å in each direction. A sp^3 carbon and a point charge of +1.0 were used as probes to generate the interaction energies at each lattice point. The default value of 30 kcal/mol was used as the maximum electrostatic and steric energy cutoff.

CoMFA calculations were then performed on the training set. The sodium channel binding activities of all compounds in the training set are listed in Table 1. These calculations generated a model with a cross-validated q^2 = 0.765 and a non-cross-validated R^2 = 0.951.

We also used the non-cross-validated CoMFA model to predict the sodium channel binding activities for the lowest energy conformations of the test set, compounds **68**–**87**, and the newly designed compounds **88**–**97**.

Table 1
The predicted and observed activities for the compounds in the training set

Compounds	Observed LogIC_{50}	Predicted LogIC_{50}	Residual
1	3.32	3.18	0.14
2	2.93	2.56	0.37
3	2.40	2.44	−0.04
4	2.40	2.31	0.09
5	2.21	2.38	−0.17
6	1.59	1.88	−0.29
7	1.11	1.31	−0.20
8	0.70	1.08	−0.38
9	0.70	0.77	−0.07
10	1.60	1.92	−0.32
11	2.40	2.56	−0.16
12	2.86	2.61	0.25
13	2.45	2.17	0.28
14	2.65	2.49	0.16
15	2.50	1.91	0.59
16	1.48	1.18	0.30
17	1.70	1.68	0.02
18	2.70	2.66	0.04
19	2.05	2.11	−0.06
20	1.11	1.13	−0.02
21	1.10	1.12	−0.02
22	0.95	1.29	−0.34
23	0.81	0.97	−0.16
24	1.92	1.77	0.15
25	1.48	1.69	−0.21
26	0.70	1.03	−0.33
27	1.54	1.33	0.21
28	0.72	1.00	−0.28
29	0.91	0.87	0.04
30	0.40	0.50	−0.10
31	0.80	0.89	−0.09
32	0.68	0.55	0.13
33	0.52	0.37	0.15
34	0.11	0.05	0.06
35	0.84	0.78	0.06
36	0.71	0.57	0.12
37	0.63	0.71	−0.08
38	−0.08	−0.18	0.10
39	0.85	0.80	0.05
40	−0.35	−0.31	−0.04
41	1.57	1.66	−0.09
42	−0.22	−0.33	0.11
43	0.55	0.85	−0.30
44	−0.56	−0.69	0.13
45	0.56	0.47	0.09
46	1.57	1.40	0.17
47	1.41	0.96	0.45
48	1.56	1.53	0.03
49	−0.52	−0.34	−0.18
50	0.52	0.53	−0.01
51	1.34	1.47	−0.13
52	1.08	1.44	−0.36
53	2.86	2.61	0.25
54	0.73	0.92	−0.19
55	1.69	1.67	0.02
56	0.78	1.28	−0.50
57	0.15	0.09	0.06
58	0.54	0.47	0.07
59	1.68	1.68	0.00
60	2.28	2.04	0.24
61	1.11	1.10	0.01
62	1.73	1.62	0.11
63	2.04	1.90	0.14
64	1.19	1.10	0.08
65	2.30	2.53	−0.23
66	0.53	0.51	0.02
67	0.59	0.83	−0.24

q^2 = 0.765 for crossvalidation; r^2 = 0.951 for non-crossvalidation. The optimum number of components is 5.

2.4. Chemistry

The newly generated CoMFA model was used to design a number of new compounds predicted to have potent binding affinities for the neuronal voltage-gated sodium channel. Several of these were selected for synthesis, and the methods employed are shown in Scheme 1. Compounds **88** and **89** (Scheme 1) were synthesized by reacting (3-aminopropyl)benzene with the appropriate alkyl chloride in DMSO at room temperature. Compounds **90** and **91** were synthesized in the same manner starting with (2-aminoethyl)benzene. Compounds **92**–**97** (Scheme 1) were synthesized by reacting *N*-(diphenylmethyl)piperazine with the appropriate halide at 70–80 °C in DMSO.

3. Results and discussion

3.1. Basic features of the model

The CoMFA calculation was carried out for the training set containing the 67 compounds. A very good correlation with a cross-validated q^2 = 0.765 and a non-cross-validated R^2 = 0.951 was achieved. The predicted and observed log IC_{50} values for the compounds in the training set are listed in Table 1. As shown in Figure 2, the correlation between the predicted and the observed values is excellent, with a correlation coefficient R^2 = 0.946 (obtained from a regression analysis by Sigmaplot, and slightly different from the non-cross-validated R^2 = 0.951 obtained from the CoMFA calculation).

The steric and electrostatic properties of the CoMFA model are illustrated separately as stereoviews in Figures 3 and 4, respectively. Compared to the known models,[25,27,28] the new model is much richer in spatial information regarding steric and electrostatic factors for the binding of ligands to the sodium channel, as evidenced by the maps of either steric or electrostatic influences on activity. Figure 3 describes the steric map, and yellow contours represent the steric limit occupied by good ligands (additional steric occupancy beyond this contour is unfavorable), while green regions represent areas where increased steric effects are favorable. Thus Figure 3 reveals one major steric region, near the *n*-alkyl group of **32**, where additional steric bulk is favorable. Regarding the electrostatic properties in Figure 4, the model reveals a major favorable positively charged region in the central part of the map, and several favorable negatively charged regions. The major positively charged region is nicely occupied by the piperazine nitrogens of **32**.

3.2. The predictive ability of the comprehensive model

To test the predictive ability of this new CoMFA model, a test set containing 20 compounds (**68**–**87**), all sodium channel blockers with known activity that were not used in the training set, was constructed. The structures of these compounds are shown in Figure 5. These compounds were selected from the same literature reference[35] that was used to provide some of our training set compounds, which can limit errors caused by different testing methodologies.

Both our current and previously published CoMFA models[25] were used to predict the sodium channel binding activities for the compounds in the test set. The results are listed in Table 2. From the results it is clear that the current model provides significantly better predictive ability than the old model for most compounds in the test set. For example, test set compound **77** had an experimentally measured log IC_{50} = −0.22, while the old model gave a predicted log IC_{50} = 0.75 (residual = −0.97) and the new model gave a predicted log IC_{50} = 0.09 (residual = −0.31). As true for **77**, most compounds in the test set had much greater accuracy of prediction by the new model as compared to the old model. Of the 20 compounds in the test set, activities for only **68**, **72**, and **81** were better predicted by the old model versus the new one.

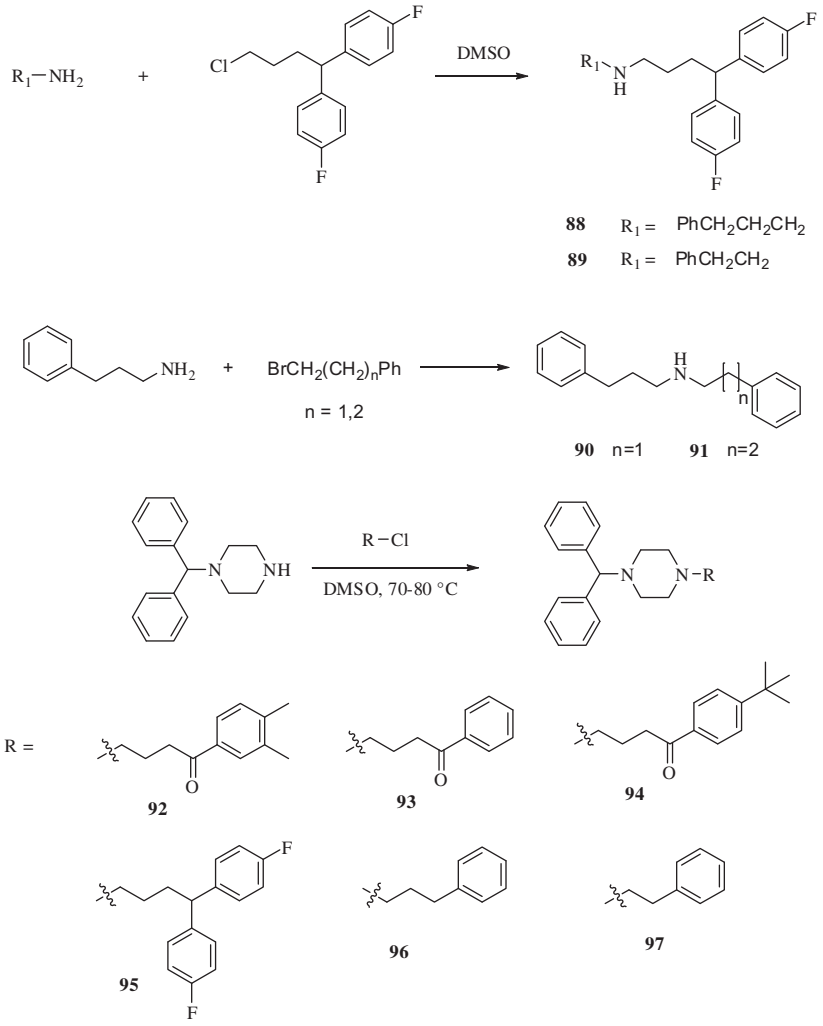

Scheme 1. Synthesis of newly designed ligands.

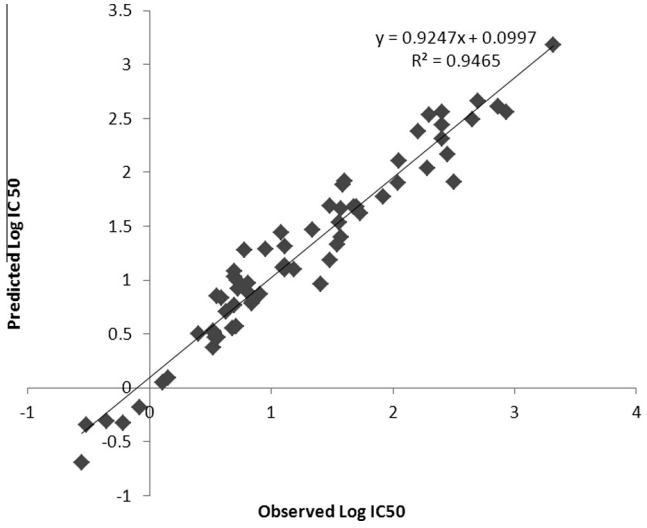

Figure 2. The correlation between the predicted and the observed activities for the training set.

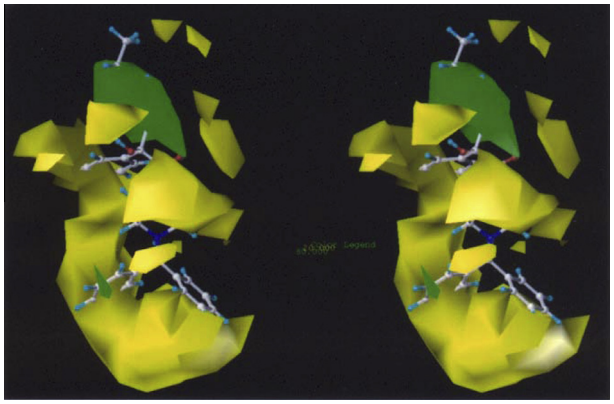

Figure 3. Stereoview for compound **32** posed in the steric map of the CoMFA model. Green: increased steric bulk here results in increased activity; Yellow: limit of steric space. Increased bulk here decreases activity. For **32**, the *n*-C_5H_{11} alkyl group at the 'top' occupies a sterically favorable region, while the remainder of **32** fills much of the available favorable steric space.

3.3. Design of new, potent sodium channel ligands

In order to use the current CoMFA model to design new compounds, we employed a 'computational SAR' approach, where systematic changes were made on structural templates that contained favorable features of the CoMFA model. The model was then used to predict the effect on activity for subtle changes in presentation of charge and steric effects for each hypothetical new

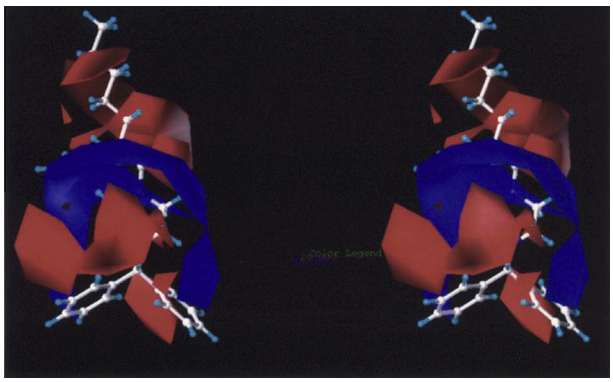

Figure 4. Stereoview for compound **32** posed in the electrostatic map of the CoMFA model. Blue: region where positive (+) charge increases activity; Red: region where negative (−) charge increases activity. The piperazine nitrogens of compound **32** occupy favorable positively charged areas near the central region of the map.

compound. For example, many of the more potent compounds contained the diphenylmethylamino fragment, and the CoMFA steric model (Fig. 3) suggested that steric bulk at each end of a ligand such as **32** is favorable. As shown in Table 3, in one SAR study we utilized a simple template containing these features and systematically varied the length of the linker between the two hydrophobic end groups (compounds **SAR-1**–**SAR-6**). This revealed a chain length optimum at $n = 5$. Similarly, we explored a variety of other structural effects, including the location, nature, and number of positive charges within the structure, and the size, nature, and location of various hydrophobic groups, among others.

Based on the information revealed by these types of studies, we designed several new sodium channel ligands that were subsequently synthesized, compounds **88**–**97**. Their structures and the synthetic procedures employed are shown in Scheme 1, and the observed and predicted IC_{50} values are given in Table 4. Several of these contained the *N*-diphenylmethylpiperazine fragment, but we also focused on simpler structures. These newly designed compounds (**88**–**97**) were predicted by the model to span a range of IC_{50} values from 251 to 1000 nM. The experimentally determined IC_{50} values in most cases were well predicted by the model, and the prediction in general did not differ from the observed value by more than 2-fold (with the exception of **90**).

Similar to cinnarizine (**40**), a nanomolar compound used in the training set for the CoMFA calculation, compounds **92**–**97** in Table 4

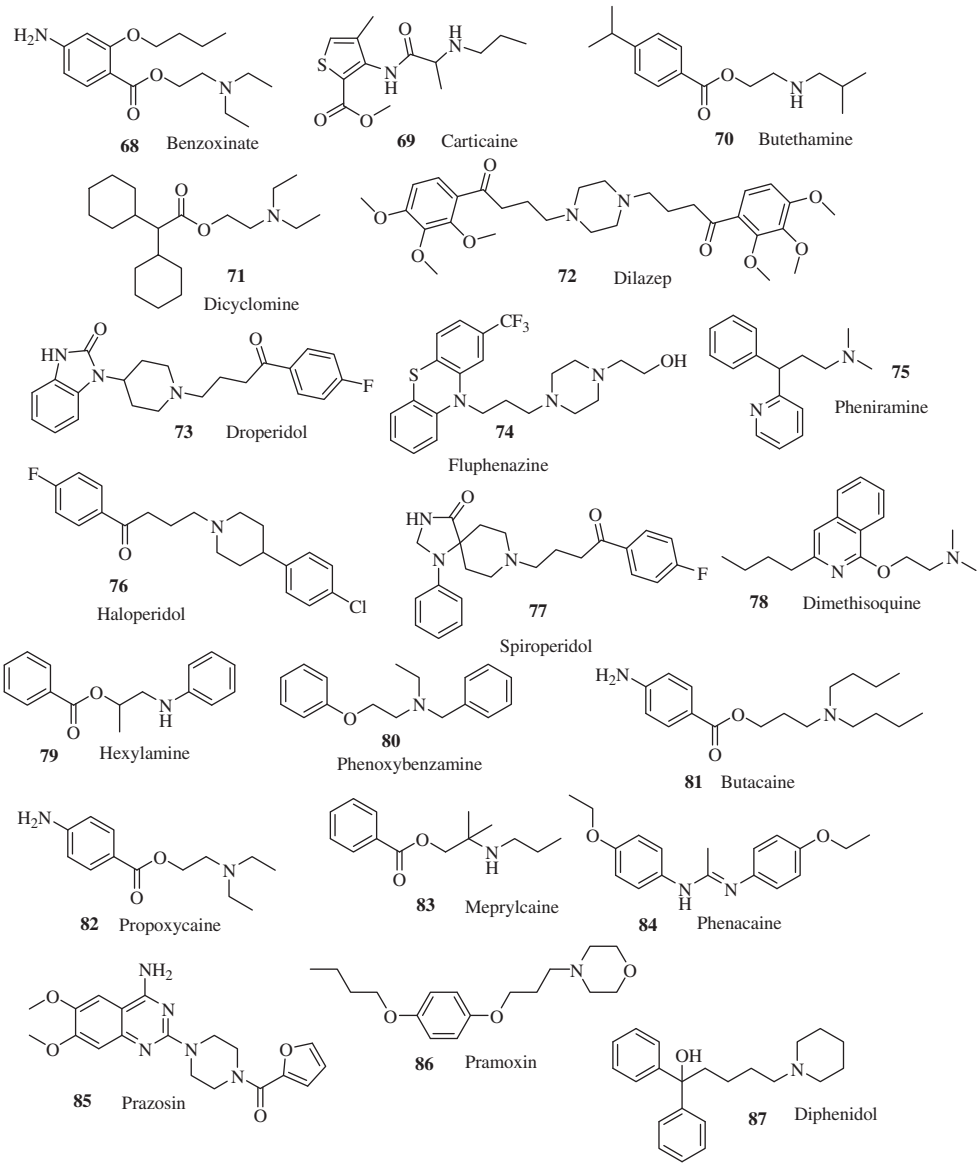

Figure 5. Compounds used in the test set.

Table 2
The predicted activity and actual activity for compounds in the test set by the old model[25] and current model

Compound	Observed Log IC_{50}	Current model		Old model	
		Predicted Log IC_{50}	Residual	Predicted Log IC_{50}	Residual
68	0.46	0.60	−0.16	0.52	−0.06
69	1.71	1.63	0.08	2.13	−0.42
70	1.74	0.94	0.80	0.53	1.21
71	0.45	0.48	−0.03	1.19	−0.74
72	−0.22	0.26	−0.48	0.07	−0.29
73	−0.13	0.50	−0.63	0.90	−1.03
74	0.57	0.01	0.56	0.02	0.55
75	1.52	1.78	−0.26	2.18	−0.66
76	0.08	0.25	−0.17	0.89	−0.81
77	−0.22	0.09	−0.31	0.75	−0.97
78	0.53	1.02	−0.49	1.82	−1.29
79	0.85	0.86	−0.01	1.19	−0.34
80	1.65	1.84	−0.19	0.83	0.82
81	0.43	0.54	−0.11	0.44	−0.01
82	1.38	1.16	0.22	0.72	0.66
83	0.88	0.93	−0.05	0.93	−0.05
84	0.23	0.64	−0.41	1.29	−1.06
85	1.33	1.24	0.09	1.44	−0.11
86	1.00	1.19	−0.19	2.41	−1.41
87	0.53	0.82	−0.19	1.07	−0.54

Correlation: current model, $Y = 0.69X + 0.32$, $r^2 = 0.718$; old model, $Y = 0.41X + 0.76$, $r^2 = 0.16$.

Table 3
The predicted effect (CoMFA) of number of atoms between the diphenylmethylamino group and a second hydrophobic group

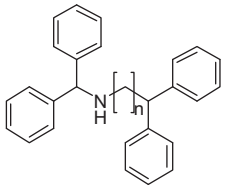

Compound	*n*	IC_{50} (nM)_
SAR-1	1	3160
SAR-2	2	760
SAR-3	3	1330
SAR-4	4	562
SAR-5	5	345
SAR-6	6	560

Table 4
The observed and the predicted ic_{50} values for newly designed compounds synthesized in Schemes 1

Compound	Predicted IC $_{50}$ (nM)	Observed IC_{50} (nM)
88	360	229 [104–382][a]
89	801	1230 [506–2200]
90	1000	340 [200–500]
91	443	252 [96–420]
92	280	156 [82–240]
93	283	283 [192–420]
94	251	128 [56–260]
95	260	119 [45–198]
96	340	192 [106–340]
97	470	257 [120–446]

[a] Numbers in brackets represent ±1 stand deviation.

all contain the diphenylmethylpiperazine fragment. While these compounds are all potent sodium channel ligands, of greater interest are the structurally much simpler compounds, **88**–**91**, we designed that do not contain this moiety. Of these, compounds **88**, **90**, and **91** are low nanomolar (nM) ligands. The simplest was compound **90**, which is a dialkylamine containing only one phenyl group at each end. To the best of our knowledge, compound **90** is among the smallest known low nM blockers of this channel.

In summary, a high-quality comprehensive 3-D QSAR (CoMFA) model was generated by using a training set of 67 sodium channel ligands (36 synthesized in this laboratory and 31 selected from the literature). This is the first published 3D-QSAR model for this target that allows design of low nM ligands. The newly generated CoMFA model was used to guide design for new sodium channel ligands predicted to have nanomolar IC_{50} values, and several structurally simple examples were synthesized. The IC_{50} values were well predicted by the model, suggesting the potential of this and related models for guiding the design of new sodium channel ligands that are potential drugs with applications in epilepsy, neuroprotection, analgesia, arrhythmias, and/or metastatic cancer.

4. Experimental section

Melting points were recorded on an Electrothermal melting point apparatus and are uncorrected. IR spectra were recorded on Bruker Vector 22 and Arid-Zone™ Bomem MB-series spectrometers. Elemental analyses were performed by Atlantic Microlabs of Norcross, GA. ^1H and ^{13}C NMR spectra were recorded on a Bruker (ARX series) NMR spectrometer operating at 300.1 MHz (for ^1H), and 75.4 MHz (for ^{13}C). The MS spectra were recorded on a Perkin-Elmer SCIEX API triple-quadrupole mass spectrometer using electrospray ionization. Analytical chromatography was performed using Whatman PE Sil G/UV silica gel plates (250 μm). Flash chromatography was performed on J.T. Baker silica gel (40 μm). All commercially obtained reagents were used as received unless otherwise noted.

4.1. General procedure for the preparation of compounds 88–91

To a solution of alkylamine (2 eqs) in DMSO (10 mL) was added the appropriate alkyl halide (1 equiv). The mixture was stirred at room temperature for 12 h until the halide disappeared from TLC. Ethyl acetate (100 mL) was added and the mixture was washed with 5% Na_2CO_3 (3 × 30 mL). The organic layer was dried (Na_2SO_4) and evaporated to give a crude product, which was purified on a silica gel column (40% ethyl acetate/55% hexanes/5% Et_3N). In this manner were prepared the following compounds.

4.2. 5,5-Di-(4-fluorophenyl)-*N*-(3-phenylpropyl)pentanamine (88)

From 3-phenylpropylamine (0.482 g, 3.56 mmol), and 4,4-di-(4-fluorophenyl)butyl chloride (0.500 g, 1.72 mmol) was prepared **88** (0.488 g, 75%) as a thick liquid (R_f = 0.65). ^1H NMR ($CDCl_3$) δ 7.29–6.91 (m, 13H, 3Ph), 3.85 (t, J = 7.5 Hz, 1H, C<u>H</u>$(PhF)_2$), 2.66–2.57 (m, 6H, C<u>H_2</u>NHC<u>H_2</u> & C<u>H_2</u>Ph), 2.03–1.96 (m, 2H, CH_2C<u>H_2</u>CH$(PhF)_2$), 1.83–1.73 (m, 2H, C<u>H_2</u>CH_2Ph), 1.46–1.36 (m, 3H, NH & C<u>H_2</u>CH_2-CH$(Ph(F))_2$); ^{13}C NMR ($CDCl_3$) δ 163.4, 160.0, 142.1, 140.8, 140.7, 129.5, 129.4, 128.8, 128.7, 126.3, 115.8, 115.5, 50.0, 49.5, 49.2, 33.89, 33.86, 31.1, 28.0; MS 380 $(M+1)^+$; IR 3058 (N-H) cm^{-1}; Anal. Calcd for $C_{22}H_{29}N$: C, 79.13; H, 7.17; N, 3.69. Found: C, 79.39; H, 7.19; N, 3.75.

4.3. 4,4-Di-(4-fluorophenyl)-*N*-(2-phenylethyl)butanamine (89)

From 2-phenylethylamine (0.180 g, 1.49 mmol) and 2-phenylethyl bromide (0.174 g, 0.620 mmol) was prepared **89** (0.192 g, 85%) as a liquid (R_f = 0.35): ^1H NMR ($CDCl_3$) δ 7.25–6.82 (m, 13H,

3Ph), 5.91 (s, 2H, NH_2^+), 3.75 (t, 1H, C<u>H</u>Ph_2), 2.89–2.76 (m, 4H, 2NC<u>H_2</u>), 2.65 (t, 2H, PhC<u>H_2</u>), 1.96–1.87 (m, 2H, C<u>H_2</u>CHPh_2), 1.47–1.38 (m, 2H, C<u>H_2</u>CH_2CHPh_2); ^{13}C NMR ($CDCl_3$) δ 163.4, 160.2, 140.7, 140.6, 129.5, 129.4, 129.1, 129.0 127.0, 115.9, 115.6, 50.4, 49.9, 48.9, 35.1, 33.7, 27.1; MS 366 $(M+1)^+$; IR 3040 (N-H), 2936 (Ar-H) cm^{-1}; Anal. Calcd for $C_{24}H_{25}NF_2$: C, 75.17; H, 7.10; N, 3.65. Found: C, 74.90; H, 6.96; N, 3.73.

4.4. *N*-(2-Phenylethyl)-3-phenylpropanamine (90)[36]

From 3-phenylpropylamine (0.180 g, 1.33 mmol) and 2-phenylethyl bromide (0.103 g, 0.556 mmol) was prepared **90** (0.130 g, 78%) as a liquid (R_f = 0.45): ^{1}H NMR ($CDCl_3$) δ 9.12 (s, 2H, NH_2^+), 7.23–7.05 (m, 10H, 2Ph), 2.73 (t, 4H, 2NC<u>H</u>$_2$), 2.56 (t, 4H, 2PhC<u>H_2</u>), 1.97–1.87 (m, 2H, $PhCH_2$C<u>H_2</u>CH_2); ^{13}C NMR ($CDCl_3$) δ; MS 240 $(M+1)^+$; IR 3061 (N-H), 2946 (Ar-H) cm^{-1}.

4.5. *N,N*-Di-(3-phenylpropyl)amine (91)[36]

From 3-phenylpropylamine (0.180 g, 1.33 mmol) and 3-phenylpropyl bromide (0.110 g, 0.552 mmol) was prepared **91** (0.077 g, 55%) as a liquid (R_f = 0.43): ^{1}H NMR ($CDCl_3$) δ 9.09 (s, 2H, NH_2^+), 7.39–7.22 (m, 10H, 2Ph), 2.86 (t, 4H, 2NC<u>H</u>$_2$), 2.69 (t, 4H, 2PhC<u>H_2</u>), 2.12–2.02 (m, 4H, $2PhCH_2$C<u>H_2</u>); ^{13}C NMR ($CDCl_3$) δ 141.0, 128.9, 128.7, 126.6, 47.8, 33.4, 28.6; MS 254 $(M+1)^+$; IR 3066 (N-H), 2931 (Ar-H) cm^{-1}.

4.6. General procedure for the preparation of 1-alkyl-4-(diphenylmethyl)piperazine

To the solution of diphenylmethyl piperazine in DMSO (8 mL) was added alkyl halide. The mixture was stirred at 70–80 °C for 10 h. The reaction mixture was transferred to a 250-mL separatory funnel, ethyl acetate (100 mL) was added, and the mixture was washed with 5% Na_2CO_3 (2 × 30 mL), water (2 × 50 mL) and brine (50 mL). The organic layer was dried (Na_2SO_4) and evaporated to dryness to give a crude product. The residue was purified by flash silica gel chromatography to afford pure product. In this manner were prepared the following compounds.

4.7. 1-[4-(3,4-Dimethylphenyl)-4-oxobutyl]-4-(diphenylmethyl)piperazine (92)

From 4-chloro-1-(3,4-dimethylphenyl)-1-butanone (1.00 g, 4.75 mmol) and 1-diphenylmethylpiperazine (2.20 g, 8.73 mmol) was prepared **92** (1.30 g, 70%) as a white solid (solvent for column: 90% hexanes + 8% ethyl acetate + 2% triethylamine, R_f = 0.65). The amine was dissolved in ethyl acetate (10 mL), and into the ethyl acetate solution was bubbled HCl gas. The solvent was removed, and the residue was recrystallized from ethanol/benzene to give a white solid (0.49 g): mp 185–187 °C; ^{1}H NMR (DMSO-d_6) δ 10.35 (b, 1H, NH^+), 7.75–7.20 (m, 13H, 3Ph), 4.48 (s, 1H, $CHPh_2$), 3.49–3.45 (d, J = 12 Hz, 2H, H^+N(C<u>H</u>)$_2$(CH_2)$_2$N), 3.16–2.85 (m, 6H, N(CH)$_2$(C<u>H_2</u>)$_2$NC<u>H_2</u>), 2.85–2.81 (d, J = 12 Hz, 2H, N(C<u>H</u>)$_2$(CH_2)$_2$N), 2.44–2.36 (m, 2H, $NHCH_2$C<u>H_2</u>CH_2), 2.29 (s, 6H, 2Me), 2.20–2.08 (m, 2H, $NHCH_2CH_2$C<u>H_2</u>). ^{13}C NMR ($CDCl_3$) δ 198.7, 143.7, 141.9, 137.5, 134.5, 130.4, 129.5, 129.3, 128.0, 126.1, 75.5, 56.8, 62.6, 48.7, 35.6, 31.3, 20.5, 20.2, 18.4; IR 1682 (C=O) cm^{-1}; MS 427 $(M+1)^+$; Anal. Calcd for $C_{29}H_{34}N_2O*HCl*H_2O$: C, 72.40; H, 7.75; N, 5.82; Cl, 7.37. Found: C, 72.73; H, 7.73; N, 5.82; Cl, 7.42.

4.8. 1-[2-(*N*-Benzoylamino)ethyl]-4-(diphenylmethyl)-1-piperazine (93)

From *N*-2-chloroethylbenzamide (1.00 g, 5.45 mmol) and 1-diphenylmethylpiperazine (2.39 g, 10.9 mmol) was prepared **93** (1.40 g, 64%) as a white solid (solvent for column: 90% hexanes + 8% ethyl acetate + 2% triethylamine, R_f = 0.40): mp 101–103 °C; ^{1}H NMR ($CDCl_3$) δ 7.77–7.18 (m, 15H, 3Ph), 6.87 (s, 1H, N<u>H</u>CO), 4.23 (s, 1H, C<u>H</u>Ph_2), 3.55–2.50 (m, 2H, C<u>H_2</u>NHCO), 2.62–2.44 (m, 10H, N(C<u>H_2</u>)$_2$(C<u>H_2</u>)$_2$NC<u>H_2</u>); ^{13}C NMR ($CDCl_3$) δ 167.4, 142.7, 134.7, 131.3, 128.5, 127.9, 127.0, 126.9, 76.3, 56.3, 53.1, 52.0, 36.3; IR 3334 (N-H), 1639 (C=O) cm^{-1}; MS 400 $(M+1)^+$; Anal. Calcd for $C_{26}H_{28}N_3O$: C, 78.16; H, 7.32; N, 10.52. Found: C, 78.00; H, 7.27; N, 10.29.

4.9. 1-(4-(4-*t*-Butylphenyl)-4-oxobutyl)-4-(diphenylmethyl)-piperazine (94)

From 4-chloro-1-(4-*t*-butylphenyl)-1-butanone (0.500 g, 2.09 mmol) and 1-(diphenylmethyl)piperazine (1.20 g, 4.76 mmol) was prepared **94** (0.488, 51%) (solvent for column: 90% hexanes + 8% ethyl acetate + 2% triethylamine, R_f = 0.60) as a thick liquid. ^{1}H NMR ($CDCl_3$) δ 7.90–7.88 (2H, Ph), 7.47–6.91 (m, 12H, 3Ph), 4.18 (s, 1H, C<u>H</u>Ph_2), 2.96 (t, J = 7.2 Hz, 2H, C<u>H_2</u>CO), 2.46–2.27 (m, 10H, N(C<u>H_2</u>)$_2$(C<u>H_2</u>)$_2$NC<u>H_2</u>), 2.20–1.96 (m, 2H, C<u>H_2</u>CH_2CO), 1.34 (s, 9H, *t*-Bu); ^{13}C NMR ($CDCl_3$) δ 200.1, 157.0, 143.2, 134.9, 128.9, 128.5, 128.3, 127.3, 125.9; MS 456 $(M+1)^+$; IR 1683 (C=O) cm^{-1}; Anal. Calcd for $C_{31}H_{38}N_2O_2$: C, 81.90; H, 8.42; N, 6.16. Found: C, 82.00; H, 8.53; N, 6.21.

4.10. 1-[4,4-Bis(4-flurophenyl)]butyl-4-(diphenylmethyl)piperazine (95)

From 1,1′-(4-chlorobutylidene)-bis-(4-fluorobenzene) (0.500 g, 1.78 mmol) and 1-(diphenylmethyl)piperazine (1.00 g, 3.97 mmol) was prepared **95** (0.755 g, 85%) (solvent for column: 68% hexanes + 30% ethyl acetate + 2% triethylamine, R_f = 0.50) as a white solid: mp 118–120 °C; ^{1}H NMR ($CDCl_3$) δ 7.40–6.90 (m, 18H, 4Ph), 4.19 (s, 1H, C<u>H</u>Ph_2), 3.85 (t, J = 7.8 Hz, 1H, C<u>H</u>(PhF)$_2$), 2.39–2.30 (m, 10H, N(C<u>H_2</u>)$_2$(C<u>H_2</u>)$_2$NC<u>H_2</u>), 2.01–1.93 (q, J = 7.8 Hz, 2H, C<u>H_2</u>CH(PhF)$_2$), 1.44–1.35 (m, 2H, C<u>H_2</u>CH_2CH(Ph(F))$_2$); ^{13}C NMR ($CDCl_3$) δ 162.9, 159.7, 142.8, 140.6, 129.1, 129.0, 128.4, 127.9, 126.9, 115.4, 115.1, 76.3, 58.5, 53.5, 51.9, 49.7, 33.9, 25.3; MS 497 $(M+1)^+$; IR 2930 (Ar-H) cm^{-1}; Anal. Calcd for $C_{33}H_{34}F_2N_2$: C, 79.81; H, 6.90; N, 5.64. Found: C, 79.79; H, 6.93: N, 5.67.

4.11. 1-(Diphenylmethyl)-4-(3-phenylpropyl)piperazine (96)

From 3-phenylpropyl bromide (0.120 g, 0.61 mmol) and 1-(diphenylmethyl)piperazine (0.360 g, 1.43 mmol) was prepared **96** (0.185 g, 81%) (solvent for column: 78% hexanes + 20% ethyl acetate + 2% triethylamine, R_f = 0.45) as a white solid: mp 83–85 °C; ^{1}H NMR ($CDCl_3$) δ 7.46–7.20 (m, 15H, 3Ph), 4.27 (s, 1H, C<u>H</u>Ph_2), 2.74–2.46 (m, 12H, N(C<u>H_2</u>)$_2$(C<u>H_2</u>)$_2$NC<u>H_2</u> & C<u>H_2</u>Ph_2), 1.90–1.80 (m, 2H, C<u>H_2</u>CH_2Ph); ^{13}C NMR ($CDCl_3$) δ 143.4, 142.7, 129.0, 128.9, 128.8, 128.5, 127.4, 76.8, 58.6, 54.0, 52.5, 34.3, 29.2; IR 3031 (Ar-H) cm^{-1}; MS 371 $(M+1)^+$; Anal. Calcd for $C_{26}H_{30}N_2$: C, 84.28; H, 8.16; N, 7.56. Found: C, 84.19; H, 8.11; N, 7.69.

4.12. 1-(Diphenylmethyl)-4-(2-phenylethyl)piperazine (97)

From 3-phenylethyl bromide (0.249 g, 1.36 mmol) and 1-(diphenylmethyl)piperazine (0.343 g, 1.36 mmol) was prepared **97** (0.170 g, 35%) (solvent for column: 88% hexanes + 10% ethyl acetate + 2% triethylamine, R_f = 0.25) as a white solid: mp 127–129 °C; ^{1}H NMR ($CDCl_3$) δ 7.48–7.21 (m, 15H, 3Ph), 4.28 (s, 1H, C<u>H</u>Ph_2), 2.85-2.53 (m, 12H, N(C<u>H_2</u>)$_2$(C<u>H_2</u>)$_2$NC<u>H_2</u> & C<u>H_2</u>Ph_2); ^{13}C NMR ($CDCl_3$) δ 143.2, 140.8, 129.1, 128.9, 128.8, 128.3, 127.3, 126.5, 76.6, 60.9, 53.9, 52.2, 34.00; IR 3030 (Ar-H) cm^{-1}; MS 357 $(M+1)^+$; Anal. Calcd for $C_{25}H_{28}N_2$: C, 84.23; H, 7.92; N, 7.86. Found: C, 84.03; H, 8.04; N, 7.78.

4.13. Sodium channel binding assay

The details for the sodium channel binding assay were reported in a previous paper.[25] Briefly, synaptoneurosomes were prepared from rat cerebral cortex as follows: Cerebral cortex slices (gray matter) were obtained by removing the white matter and other subcortical structure. The slices (about 1 g) were then homogenized in 2 mL of incubation buffer containing 130 mM choline chloride, 50 mM HEPES, 5.5 mM glucose, 0.8 mM $MgSO_4$, and 5.4 mM KCl (adjusted to pH = 7.4 with Tris base). The tissue was homogenized with 10 full strokes of a glass–glass homogenizer. The tissue preparation was then transferred to a centrifuge tube. The homogenizer was rinsed with 3 mL of the incubation buffer, which was combined with the preparation. The preparation was then centrifuged at 1000*g* for 15 min at 4 °C. The pellet was re-suspended in a total volume of 20 mL of the incubation buffer and transferred to a 50-mL homogenizer. Three full strokes were used to homogenize the tissue. The resulting suspension was then filtered, first with three layers of nylon mesh by gravity, and then with Whatman 4 filter paper by house vacuum. The filtrate was then centrifuged at 1000*g* for 30 min at 4 °C. The obtained pellet was re-suspended with 5 mL isotonic buffer, and more isotonic buffer was used as needed to adjust the suspension to have an absorbance of 1 at 280 nm. The isotonic suspension was stored in a freezer at −70 °C. Prior to the binding assay, the tissue was thawed and the suspension was centrifuged, and the pellet was re-suspended in the HEPES incubation buffer (same volume as the isotonic buffer used to store the tissue).

In the sodium channel binding assay, this suspension of synaptoneurosomes (~1 mg of protein) from rat cerebral cortex was incubated for 60 min at 25 °C with the test compound (seven different concentrations spanning the IC_{50}) in a total volume of 320 μL containing 10 nM [^{3}H]BTX-B and 50 μg/mL of scorpion venom. Incubations were terminated by dilution with ice-cold buffer and filtration through a Whatman GF/C filter paper under vacuum condition, and the filters were washed four times with ice-cold buffer. Filters were counted in a Beckman scintillation counter. Specific binding was determined by subtracting the nonspecific binding, which was measured in the presence of 300 μM veratridine, from the total binding of [^{3}H]BTX-B. All experiments were performed in triplicate and included a control tube containing 40 μM DPH. The allowed IC_{50} value of DPH was 40 ± 4 (10%) μM, and an assay would be repeated if the IC_{50} value was beyond this range, which was uncommon. The IC_{50} values of test compounds were determined from a Probit analysis of the dose–response curve and excluded doses producing less than 10% or greater than 90% inhibition.

Supplementary data

Supplementary data associated with this article can be found, in the online version, at http://dx.doi.org/10.1016/j.bmc.2013.11.049.

References and notes

1. Catterall, W. A.; Wood, J. N.; Baker, M. *Curr. Opin. Pharmacol.* **2001**, *1*, 17.
2. Catterall, W. A. *J. Bioenerg. Biomembr.* **1996**, *28*, 219.
3. Hille, B. *Ionic Channels of Excitable Membranes*; Sinauer Associates: Sunderland, MA, 1991.
4. Catteral, W. A. *Trends Neurosci.* **1986**, *9*, 7.
5. Yu, F. H.; Catterall, W. A. *Genome Biol.* **2003**, *4*, 207.
6. Taylor, C. P.; Narasimhan, L. S. *Adv. Pharmacol.* **1997**, *39*, 47.
7. Yao, C.; Williams, A. J.; Lu, X. C.; Price, R. A.; Cunningham, B. S.; Berti, R.; Tortella, F. C.; Dave, J. R. *Neurotoxicity Res.* **2003**, *5*, 245.
8. Brown, A. M.; Schwindt, P. C.; Crill, W. E. *J. Neurophysiol.* **1994**, *71*, 2562.
9. Ragsdale, D. S.; Avoli, M. *Brain Res. Rev.* **1998**, *26*, 16.
10. Campell, T. J.; Williams, K. M. *Br. J. Clin. Pharmacol.* **1998**, *46*, 307.
11. Sheldon, R. S.; Duff, H. J.; Thakore, E.; Hill, R. J. *J. Pharmacol. Exp. Ther.* **1994**, *268*, 187.
12. Urenjak, J.; Obrenovitch, T. P. *Pharmacol. Rev.* **1996**, *48*, 21.
13. Catterall, W. A. *Mol. Pharmacol.* **1981**, *20*, 356.
14. di Vadi, P. P.; Hamann, W. *Anesthesia* **1998**, *53*, 808.
15. Deffois, A.; Fage, D.; Carter, C. *Neurosci. Lett.* **1996**, *220*, 117.
16. Waxman, S. G.; Cummins, T. R.; Dib-Hall, S.; Fjell, J.; Black, J. A. *Muscle Nerve* **1999**, *22*, 1177.
17. Courtney, K. R. *J. Pharmacol. Exp. Ther.* **1980**, *213*, 114.
18. Hille, B. *J. Gen. Physiol.* **1977**, *69*, 497.
19. Fraser, S. P.; Diss, J. K.; Chioni, A. M.; Mycielska, M.; Pan, H.; Yamaci, R. F., et al *Clin. Cancer Res.* **2005**, *11*, 5381 [PubMed: 16061851].
20. Onganer, P. U.; Djamgoz, M. B. J. *Membr. Biol.* **2005**, *204*, 67.
21. Yang, M.; Kozminski, D. J.; Modak, R.; Calhoun, J. D.; Isom, L. L., et al *Breast Cancer Res. Treat.* **2012**, *134*, 603.
22. Brackenbury, W. J. *Channels (Austin)* **2012**, *6*, 352.
23. Fraser, S. P.; Salvador, V.; Manning, E. A.; Mizal, J.; Altum, S.; Raza, M., et al *J. Cell. Physiol.* **2003**, *195*, 479.
24. Abdul, M.; Hoosein, N. *Anticancer Res.* **2001**, *21*, 2045.
25. Brown, M. L.; Zha, C. C.; Van Dyke, C. C.; Brown, G. B.; Brouillette, W. J. *J. Med. Chem.* **1999**, *42*, 1537.
26. Zha, C.; Brown, G. B.; Brouillette, W. J. *J. Med. Chem.* **2004**, *47*, 6519.
27. Brown, M. L.; Eidam, H. A.; Paige, M.; Jones, P. J.; Patel, M. K. *Bioorg. Med. Chem.* **2009**, *17*, 7056.
28. Wang, Y.; Jones, P. J.; Batts, T. W.; Landry, V.; Patel, M. K.; Brown, M. L. *Bioorg. Med. Chem.* **2009**, *17*, 7027.
29. Catterall, W. A. *Trends Pharmacol. Sci.* **1987**, *8*, 57.
30. Ragsdale, D. S.; McPhee, J. C.; Scheuer, T.; Catterall, W. A. *Science* **1994**, *265*, 1724.
31. Li, H.-L.; Galue, A.; Meadows, L.; Ragsdale, D. S. *Mol. Pharmacol.* **1999**, *55*, 134.
32. Ragsdale, D. S.; McPhee, J. C.; Scheuer, T.; Catterall, W. A. *Proc. Natl. Acad. Sci. U.S.A.* **1998**, *93*, 9270.
33. Qu, Y.; Rogers, J.; Tanade, T.; Scheuer, T.; Catterall, W. A. *Proc. Natl. Acad. Sci. U.S.A.* **1995**, *92*, 11839.
34. Sheldon, R. S.; Hill, R. J.; Taouis, M.; Wilson, L. M. *Mol. Pharmacol.* **1991**, *472*, 373.
35. McNeal, E. T.; Lawandowski, G. A.; Daly, J. W.; Creveling, C. R. *J. Med. Chem.* **1985**, *28*, 381.
36. Glennon, R. A.; Alordeppey, S. Y.; Ismaiel, A. M.; El-Ashmawy, M. B.; Fisher, J. B.; Howie, K. B. *J. Med. Chem.* **1994**, *37*, 1214.